Chinese Chemical Letters 33 (2022) 2954–2958

Contents lists available at ScienceDirect

Chinese Chemical Letters

journal homepage: www.elsevier.com/locate/cclet

Novel photoelectrochemical immunosensor for MCF-7 cell detection based on n-p organic semiconductor heterojunction

Qin Zeng[a,b], Qingya Wei[a], Jiarong Luo[a], Yong Qian[c], Minghui Yang[a,*], Yingping Zou[a,*], Limin Lu[b,*]

[a] Hunan Provincial Key Laboratory of Micro & Nano Materials Interface Science, College of Chemistry and Chemical Engineering, Central South University, Changsha 410083, China
[b] Institute of Functional Materials and Agricultural Applied Chemistry, College of Science, Jiangxi Agricultural University, Nanchang 330045, China
[c] Jiangxi Key Laboratory for Mass Spectrometry and Instrumentation, East China University of Technology, Nanchang 330013, China

ARTICLE INFO

Article history:
Received 29 September 2021
Revised 25 December 2021
Accepted 31 December 2021
Available online 7 January 2022

Keywords:
Photoelectrochemical immunosensor
Organic semiconductors
n-p Heterojunction
MCF-7

ABSTRACT

In this work, we developed a novel photoelectrochemical (PEC) sensor based on n-p organic semiconductor heterojunction for sensitive detecting MCF-7 cancer cells. BTA-C4Ph and PM6 were designed as photoactive materials to form n-p heterojunction, which greatly enhanced the photoelectric conversion efficiency. Antibody-modified magnetic nanoparticles were utilized to capture and separate MCF-7 cells from samples. Detection of MCF-7 is ascribed to the loading of MCF-7 onto BTA-C4Ph-PM6 modified electrode that resulted in the decrease of photocurrent intensity. The PEC immunosensor displayed a linear concentration ranging from 50 cell/mL to 1×10^4 cell/mL with a limit of detection (LOD) of 41 cell/mL (S/N = 3) for MCF-7. Additionally, the senor also exhibited good stability, excellent selectivity and prominent reproducibility. Furthermore, the sensor was successfully applied to detect MCF-7 in whole blood. This work illustrates that n-p heterojunction of organic semiconductor may find wide applications for the preparation of different photoelectrochemical sensors.

Breast cancer is a malignant tumor with the highest incidence rate and is the second fatal rate among women [1]. Early diagnosis is the main means to reduce the mortality and morbidity of breast cancer [2]. Michigan cancer foundation-7 (MCF-7) is one type of human breast cancer cells. Currently, various analytical techniques are reported for MCF-7 detection, including differential pulse voltammetry (DPV) [3], electrochemiluminescence (ECL) [4], electrochemical impedance spectroscopy (EIS) [5,6], inductively coupled plasma-mass spectrometry (ICP-MS) [7], localized surface plasmon resonance (LSPR) spectra [8], Fluorescence spectra [9] *etc*. However, development of approach for MCF-7 detection in human blood with high selectivity and sensitivity are still highly required for early breast cancer diagnosis.

Photoelectrochemical (PEC) detection has arisen as a promising technique for detecting biomarkers owing to its simple operation and easy of miniaturization [10–12]. It also demonstrates a low background signal and high sensitivity caused by the complete isolation of exciting source and detecting signal [13,14]. Generally, the performance of PEC sensor depends heavily on the photo-to-current conversion efficiency of photoactive materials employed in the design of sensors. However, single photosensitive material often hard to satisfy the practical application due to its low efficiency for electron-hole separation [15]. Consequently, much attention has paid on two or more kinds of semiconductors forming a heterojunction nanostructure [16–19]. Compared with inorganic heterojunction, organic semiconductor heterojunction has adjustable energy level and higher matching degree, which is beneficial to improve the photoelectric conversion efficiency [20–25].

PM6 as organic semiconductor donor has high crystallinity and strong π-π stacking arrangement with the highest occupied molecular orbital (HOMO) of −5.56 eV and lowest unoccupied molecular orbital (LOMO) of −3.50 eV These characteristics are conducive to the transport of charge carriers, thereby inhibiting the recombination of electron-hole pairs [26,27]. For example, organic photovoltaics based on Y6-PM6 heterojunction can achieve a high efficiency of 15.7% [28,29]. Organic semiconductor receptors have advantages such as adjustable molecular structures, regulable energy levels and strong light absorption, which are widely used in organic solar cells. For instance, Duan *et al.* designed a solar cell module based on organic semiconductor ac-

* Corresponding authors.
E-mail addresses: yangminghui@csu.edu.cn (M. Yang), yingpingzou@csu.edu.cn (Y. Zou), lulimin816@hotmail.com (L. Lu).

https://doi.org/10.1016/j.cclet.2021.12.090
1001-8417/

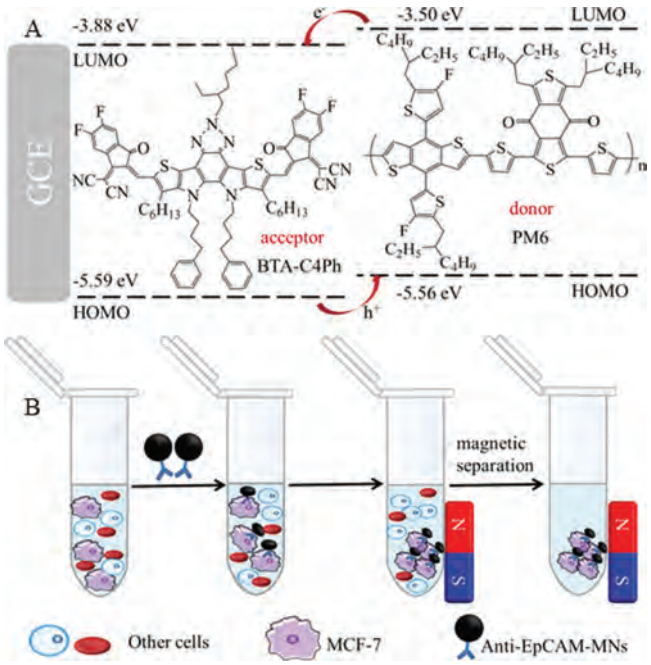

Scheme 1. (A) Electron-hole pair transfer process of BTA-C4Ph-PM6 heterojunction. (B) The process of enriching MCF-7 cells.

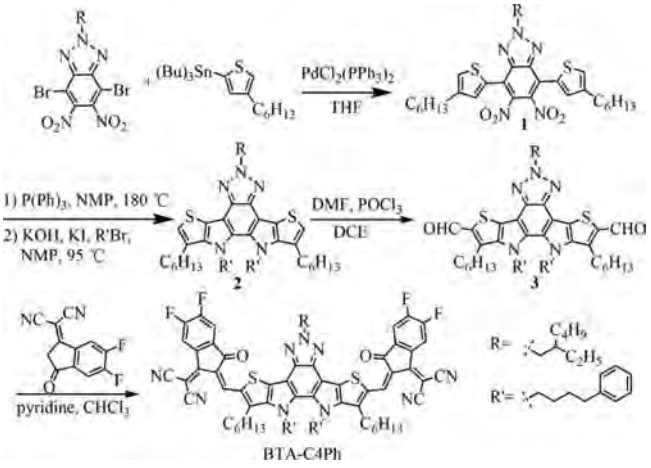

Fig. 1. The synthetic procedure of BTA-C4Ph.

ceptor N3 with power conversion efficiency average of 14.10% [21]. BTA-C4Ph is an unreported low-band gap n-type organic semiconductor acceptor, deriving from the advanced organic semiconductor material Y6 [28]. The absorption wavelength of BTA-C4Ph ranges from 500 nm to 800 nm with a HOMO of −5.59 eV and a LUMO of −3.88 eV The energy levels of BTA-C4Ph and PM6 are highly matched, indicating BTA-C4Ph-PM6 heterojunction has the potential in PEC detection.

Herein, we reported a label-free PEC immunosensor for detecting MCF-7 cells utilizing BTA-C4Ph-PM6 as the photoelectric material and magnetic nanoparticles (MNs) for capture and enrichment MCF-7 cells from blood samples (Scheme 1). BTA-C4Ph and PM6 formed an n-p heterojunction, which not only improved the photoelectric conversion efficiency of organic semiconductors, but also effectively inhibited the recombination of electron-hole pairs. The highly matched energy levels between BTA-C4Ph and PM6 resulted in a high photocurrent for the BTA-C4Ph-PM6 heterogeneity, which ensured the sensing sensitivity. MNs are nontoxic and widely used in biosensing [30]. While, MNs modified with antibodies can specifically bind to epithelial cell adhesion molecule (EpCAM) on the MCF-7 cell surface, providing high selectivity of the sensor [31–33]. With the loading of MCF-7 onto the electrode, the photocurrent intensity of the electrode is suppressed, which is proportional to cell concentration. The sensor shows high specificity, reproducibility and good stability. Furthermore, the PEC senor was successfully applied for analyzing MCF-7 in whole blood samples.

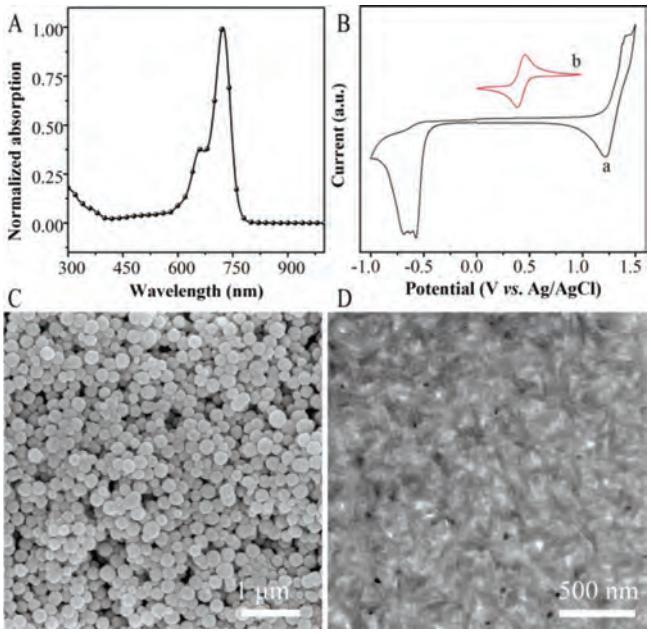

Fig. 2. (A) Normalized absorption spectra of BTA-C4Ph in the chloroform. (B) Cyclic voltammogram of BTA-C4Ph (a) and Fc/Fc^+ (b). (C) SEM image of Fe_3O_4 MNs. (D) TEM image of BTA-C4Ph-PM6.

The synthetic process of BTA-C4Ph is shown in Fig. 1. The compound **1** was prepared by Stille coupling reaction of 4,7-dibromo-2-(2-ethylhexyl)-5,6-dinitro-2*H*-benzo[*d*][1,2,3]triazole with tributyl(4-hexylthiophen-2-yl)stannane and then went through a double intramolecular Cadogan reductive cyclization and an *N*-alkylation to obtain the fused compound **2**. The compound **3** was then synthesized by the Vilsmeier-Haack reaction. The target molecule BTA-C4Ph was achieved through the Knoevenagel condensation between the compound **3** and 2-(5,6-difluoro-3-oxo-2,3-dihydro-1*H*-inden-1-ylidene)malononitrile (2FIC). The details of the synthesis procedures were shown in Supporting information. The intermediate and target materials were characterized by ^1H NMR and ^{13}C NMR, and the corresponding NMR spectra were displayed in Figs. S2-S6 (Supporting information).

To form BTA-C4Ph-PM6 heterojunction, 1 mg BTA-C4Ph and 1 mg PM6 were dispersed in 1 mL tetrahydrofuran (THF), respectively, and then mixed and sonicated for 10 min to prepare 2 mL BTA-C4Ph-PM6 heterojunction solution.

Carboxyl functionalized Fe_3O_4 nanoparticles (Fe_3O_4 MNs) were acquired by hydrothermal method on the basis of the previous reports [32–34]. The detailed procedure for synthesis of Fe_3O_4 and anti-EpCAM-MNs were shown in Supporting information.

As represented in Scheme 1B, for capture and enrich MCF-7 from samples, 100 μL anti-EpCAM-MNs (200 μg/mL) nanocomposite was added to NaCl (0.9%) solution with different concentration of MCF-7 cells. At room temperature, the reaction was shaken for 1 h. Anti-EpCAM-MNs-MCF-7 was separated by magnetic separation and re-dispersed in 1 mL NaCl (0.9%).

To prepare the PEC sensor, BTA-C4Ph-PM6 heterojunction hybrid was sonicated for 10 min, and then 10 μL BTA-C4Ph-PM6 mixed solutions was added onto the surface of cleaned GCE. Af-

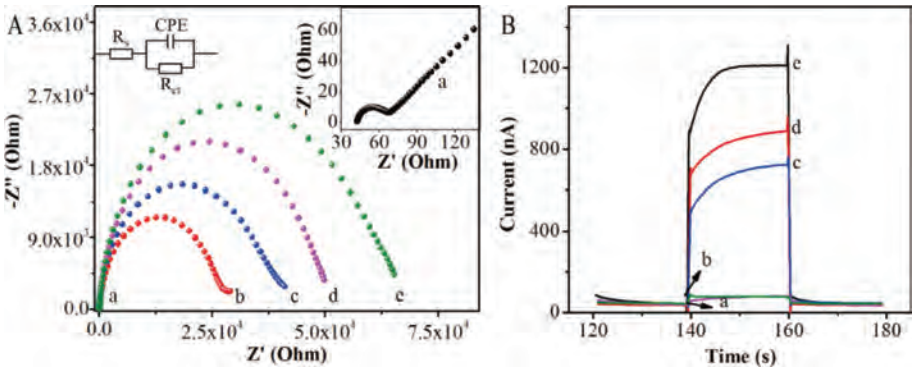

Fig. 3. (A) EIS responses of electrodes: (a) bare GCE, (b) BTA-C4Ph/GCE, (c) BTA-C4Ph-PM6/GCE, (d) BTA-C4Ph-PM6/anti-EpCAM-MNs/GCE, (e) BTA-C4Ph-PM6/anti-EpCAM-MNs/MCF-7/GCE. Supporting electrolyte: 5.0 mmol/L $K_3Fe(CN)_6/K_4Fe(CN)_6$ (1:1) containing 0.1 mol/L KCl. (B) Photoelectric responses of electrodes: (a) PM6/GCE, (b) BTA-C4Ph/GCE, (c) BTA-C4Ph-PM6/anti-EpCAM-MNs/MCF-7/GCE, (d) BTA-C4Ph-PM6/anti-EpCAM-MNs/GCE, (e) BTA-C4Ph-PM6/GCE. PEC test was in 0.01 mol/L PBS (pH 7.2~7.4) at a bias potential of −0.3 V (*vs.* Ag/AgCl) under visible light irradiation ($\lambda > 420$ nm).

ter dried under infrared light, 30 μL anti-EpCAM-MNs-MCF-7 compounds was dropped on the surface of the modified electrode, which was incubated in an oven at 37 °C for 1 h, and rinsed with DI water for testing.

The normalized absorption spectra and cyclic voltammetry (CV) curve of BTA-C4Ph were shown in Fig. 2. The absorption spectrum of BTA-C4Ph (Fig. 2A) exhibits an obvious absorption peak at around 720 nm. CV was employed to measure the electrochemical properties of BTA-C4Ph. The HOMO and LUMO energy levels can be calculated by the formula of $E_{HOMO/LUMO} = -e(4.80 - \varphi_{1/2,\ Fc/Fc^+} + \varphi_{onset,\ ox/red})$ (eV), where the $\varphi_{1/2,\ Fc/Fc^+}$ is the redox potential of Fc/Fc^+ *vs.* Ag/AgCl (0.44 V), $\varphi_{onset,\ ox/red}$ is the onset potential of oxidation (φ_{ox}) and reduction (φ_{red}) of BTA-C4Ph in the measurement system. The CV curve of BTA-C4Ph is shown in Fig. 2B. The φ_{ox} and φ_{red} are 1.23 V and -0.48 V, respectively. Consequently, the E_{HOMO}/E_{LUMO} values were calculated as −5.59/−3.88 eV.

Scanning electron microscopy (SEM) and transmission electron microscopy (TEM) were applied to study the morphology of the Fe_3O_4 MNs and BTA-C4Ph-PM6. As shown in Fig. 2C, the size of Fe_3O_4 MNs is approximate 200 nm with a classic spherical structure. Fig. 2D illustrates that the BTA-C4Ph-PM6 heterojunction displays well-defined suitable nanofiber structure, which is beneficial to the transmission of electrons [28].

The electrochemical impedance spectroscopy (EIS) was applied to characterize electrode modification process. The semicircle diameter in the Nyquist plots equals to the electron transfer resistance (Ret). Fig. 3A reveals the EIS of various modified electrodes in 5.0 mmol/L $K_3Fe(CN)_6/K_4Fe(CN)_6$ (1:1) solution containing 0.1 mol/L KCl. As can be seen, bare electrode (curve a) shows a lower Ret value. However, after the coating of BTA-C4Ph (curve b) or BTA-C4Ph-PM6 (curve c) on bare electrode, the Ret values increase significantly. This phenomenon is attributed to the semiconductor nature of the organic material as most organics are covalent compounds with no free electrons or ions, which can result in slow charge flow and weak conduct electricity. When anti-EpCAM-MNs (curve d) were immobilized on the modified electrode, Ret was further increased, revealing that anti-EpCAM-MNs hindered the electron transfer of electrode. Moreover, the incubation with MCF-7 cells (curve e) resulted in a larger Ret increase, illustrating that the cells were successfully captured by the anti-EpCAM. These results proved the successful preparation of the electrode.

The feasibility of the PEC sensor for MCF-7 detection was investigated by chronoamperometry method. Fig. 3B shows photocurrent responses of different modified electrodes in 0.01 mol/L phosphate buffered saline (PBS). As illustrated in Fig. 3B, the photocurrent response is small when mere immobilization of BTA-C4Ph

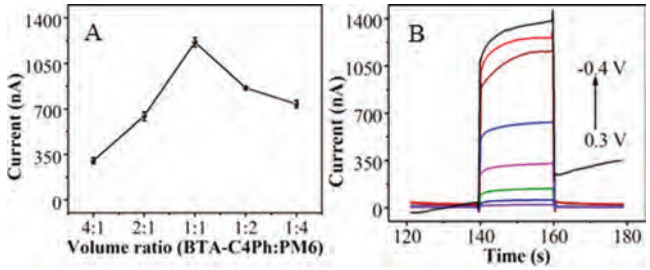

Fig. 4. (A) Photocurrent responses of electrodes modified with different volume ratios of BTA-C4Ph and PM6. (B) Photocurrent responses of electrode at different voltages. PEC test was in 0.01 mol/L PBS (pH 7.2~7.4) at a bias potential of −0.3 V (*vs.* Ag/AgCl) under visible light irradiation ($\lambda > 420$ nm).

(curve b) or PM6 (curve a) onto the electrode. In contrast, for BTA-C4Ph-PM6 heterojunction (curve e) modified electrode, the photocurrent increases significantly, which is because the electron-hole transition occurred between the acceptor BTA-C4Ph and the donor PM6. The energy level match between BTA-C4Ph and PM6 effectively inhibited the recombination of electron-hole pairs and improved the photocurrent response of single organic semiconductors. After the sequential immobilization of anti-EpCAM-MNs (curve d) and MCF-7 cells (curve c) onto the electrode, the photocurrent gradually decreased, indicating the MCF-7 cells were successfully captured by the anti-EpCAM and the feasibility of photoelectric detecting of MCF-7.

Different experimental parameters, including bias potential and volume ratio of BTA-C4Ph:PM6 were studied to acquire optimal performance for MCF-7 determination.

Fig. 4A shows the effect of the volume ratio of BTA-C4Ph (0.5 mg/mL) and PM6 (0.5 mg/mL) on the photocurrent intensity by changing the volume ratio of BTA-C4Ph to PM6 from 4:1 to 1:1, the photocurrent signal increases obviously. However, the peak current gradually decreases with further increase of the volume ratio to 1:4. This phenomenon might be related to the formation of heterojunctions between BTA-C4Ph and PM6. In the heterojunction, electrons and holes undergo transitions when exposed to light. However, excessive PM6 may lead to an imbalance in the concentration of carriers and holes produced by the heterojunction when illuminated, affecting the leap efficiency and causing a decrease in photocurrent. Therefore, volume ratio of 1:1 is chosen as the optimal volume ratio for MCF-7 detection.

The photocurrent intensity of BTA-C4Ph-PM6/GCE under different bias voltages was illustrated in Fig. 4B. The photocurrent response of BTA-C4Ph-PM6/GCE increases gradually as the change of the bias potential from 0.3 V to −0.4 V. Nevertheless, when the

Table 1
Comparison of analytical performance between the proposed PEC method and other MCF-7 sensors.

Material	Analytical methods	Analytical ranges (cell/mL)	LODs (cell/mL)	Ref.
Fe_3O_4@Ag-Pd	DPV	50×10^1–1×10^7	34	[4]
CQDs@MSNs	ECL	5×10^2–2×10^7	230	[5]
p-COF	EIS	5×10^2–1×10^5	61	[6]
CDs@ZrHf-MOF	EIS	1×10^2–1×10^5	23	[7]
MB-Apt-FAM-Au NP	ICP-MS	2×10^2–1.2×10^4	81	[8]
GNRs	LSPR	1×10^2–1×10^5	100	[9]
BTA-C4Ph-PM6	PEC	50×10^1–1×10^4	41	This work

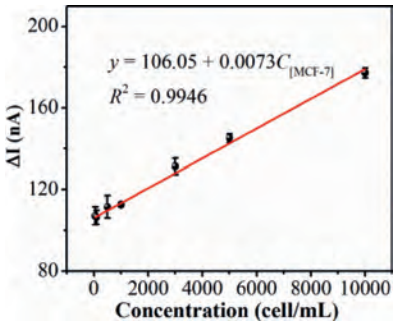

Fig. 5. The linear relationship of the photocurrent variation between BTA-C4Ph-PM6/anti-EpCAM-MNs/GCE and BTA-C4Ph-PM6/anti-EpCAM-MNs/MCF-7/GCE with MCF-7 cells concentration, error bar is SD ($n = 3$). PEC test was in 0.01 mol/L PBS (pH 7.2~7.4) at a bias potential of -0.3 V (*vs.* Ag/AgCl) under visible light irradiation ($\lambda > 420$ nm).

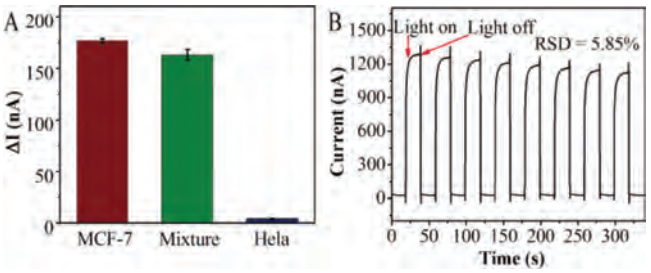

Fig. 6. (A) The selectivity of the PEC assay for determining MCF-7 cells. (B) The stability of PEC sensor. PEC test was in 0.01 mol/L PBS (pH 7.2~7.4) at a bias potential of −0.3 V (*vs.* Ag/AgCl) under visible light irradiation ($\lambda > 420$ nm).

bias voltage reaches −0.4 V, the photocurrent baseline begins to be unstable. This phenomenon is due to the fact that the applied electric field accelerates the separation and transition of electron-hole pairs. However, when the voltage is too high, the material attached on the electrode surface may fall off and affect the stability of the photocurrent. Therefore, −0.3 V is chosen as the optimum bias potential for MCF-7 detection.

With the optimal experimental conditions, the PEC sensor based on BTA-C4Ph-PM6 heterojunction was applied to detect MCF-7 and the change in photocurrent of the electrodes correlates directly with the concentration of MCF-7 cells. Fig. 5 shows the linear relation between photocurrent variation and MCF-7 cell concentration. It can be seen from the figure that as the concentration of MCF-7 cells increases, the photocurrent variation gradually increases. The linear correlation coefficient is 0.9946 within the concentration of MCF-7 in the range from 50 cell/mL to 1×10^4 cell/mL. The LOD is calculated to be 41 cell/mL ($S/N = 3$), which is lower than several articles published for MCF-7 detection (Table 1).

The selectivity of the PEC sensor was evaluated using Hela cells as control. As demonstrated in Fig. 6A, the photoelectric response to 1×10^4 cell/mL HeLa cells was very weak. However, the response signal was greatly enhanced to the mixture containing 1×10^4 cell/mL Hela cells and 1×10^4 cell/mL MCF-7 cells, which was comparable to that with only the MCF-7 cells (1×10^4 cell/mL). These phenomena demonstrate that the proposed sensor showed high selectivity for MCF-7 cancer cells.

Table 2
Determination of MCF-7 in whole blood using the PEC assay.

Sample	Added (cell/mL)	Found (cell/mL)	Recovery (%)	RSD (%)
1	500	546	109.2	1.45
2	1000	1066	108.9	3.71
3	5000	5242	104.9	5.44

To study the reproducibility of the PEC sensor, three sensors were prepared for the detection of 1×10^4 cell/mL MCF-7. The RSD is 1.19%, indicating good reproducibility. Moreover, the stability of the PEC assay was researched by continuous 'on-off' irradiation under a xenon lamp. As shown in Fig. 6B, after 8 consecutive on-off cycles of irradiation, the background photocurrent was basically unchanged with RSD of 5.85%, indicating that the PEC sensor has good stability.

To assess the applicability of the sensor, the PEC sensor was used to determine MCF-7 cells in whole blood with a standard addition method. Whole blood samples were obtained from the Xiangya Hospital and diluted 8-fold without any other treatment. Specific amounts of MCF-7 cells (5×10^2, 1×10^3, 5×10^3 cell/mL) were then added to these whole blood samples. Each sample was tested three times ($n = 3$). The results were shown in Table 2. The recoveries were within 104.9% and 109.2% with RSDs in the range of 1.45% to 5.44%. The results show that the PEC sensor can specifically detect MCF-7 in whole blood, which has potential application value.

In summary, a novel photoelectrochemical immunosensor was reported for the sensitive determination of MCF-7, where BTA-C4Ph-PM6 heterojunction served as photoelectric active materials. BTA-C4Ph-PM6 heterojunction improved the photoelectric conversion efficiency of single organic semiconductors, which enhanced the PEC current intensity. Anti-EpCAM-MNs nanocomposite was used to recognize the EpCAM protein on the surface of MCF-7 cells to achieve the separation and enrichment of MCF-7 cells. Based on these advantages, the PEC sensor provides a linear response ranging from 50 cell/mL to 1×10^4 cell/mL with a limit of detection (LOD) of 41 cell/mL ($S/N = 3$). This work paved a new way for application of organic heterojunction in preparation of PEC sensors, which may find wide application in different areas.

Declaration of competing interest

The authors declare that they have no known competing financial interests or personal relationships that could have appeared to influence the work reported in this paper.

Acknowledgments

The authors are thankful for the support of this work by the National Natural Science Foundation of China (No. 22174163), the

Hunan Provincial Science and Technology Plan Project, China (No. 2019TP1001), and the Innovation Driven Project of Central South University (No. 2020CX002).

Supplementary materials

Supplementary material associated with this article can be found, in the online version, at doi:10.1016/j.cclet.2021.12.090.

References

[1] R.L. Siegel, K.D. Miller, H.E. Fuchs, CA Cancer. J. Clin. 71 (2021) 7–33.
[2] D. Roder, N. Houssami, G. Farshid, et al., Breast Cancer. Res. Treat. 108 (2008) 409–416.
[3] T.T. Zheng, Q.F. Zhang, S. Feng, et al., J. Am. Chem. Soc. 136 (2014) 2288–2291.
[4] M. Su, H. Liu, L. Ge, Electrochimica. Acta 146 (2014) 262–269.
[5] X. Yan, Y.P. Song, J.M. Liu, et al., Biosens. Bioelectron. 126 (2019) 734–742.
[6] C.X. Gu, C.P. Guo, Z.Z. Li, et al., Biosens. Bioelectron. 134 (2019) 8–15.
[7] B. Yang, B.B. Chen, M. He, et al., Anal. Chem. 90 (2018) 2355–2361.
[8] Y. Li, Y.L. Zhang, M. Zhao, et al., Chem. Commun. 52 (2016) 3959–3961.
[9] Z.Q. Liang, Y.Q. Sun, R.H. Duan, et al., Anal. Chem. 93 (2021) 12434–12440.
[10] D. Wu, Z.H. Zhang, Chem. Commun. 55 (2019) 14514–14517.
[11] J. Wang, J. Long, Z.H. Liu, Biosens. Bioelectron. 91 (2017) 53–59.
[12] J.F. Chang, W.X. Lv, J.H. Wu, et al., Chin. Chem. Lett. 32 (2021) 775–778.
[13] H. Dai, S. Zhang, Z. Hong, et al., Anal. Chem. 88 (2016) 9532–9538.
[14] D. Jiang, X. Du, L. Zhou, et al., Anal. Chem. 89 (2017) 4525–4531.
[15] G.L. Wang, J.J. Xu, H.Y. Chen, Sci. China. Chem. 52 (2009) 1789–1800.
[16] N. Kodan, M. Ahmad, B.R. Mehta, Int. J. hydrogen. Energy. 46 (2021) 189–196.
[17] K. Zou, Y.M. Fu, R.Y. Yang, et al., Anal. Chim. Acta 1099 (2020) 75–84.
[18] Q.W. Chen, C. Yuan, C.Y. Zhai, et al., Chin. Chem. Lett. 33 (2021) 983–986.
[19] D. Long, M.j. Li, H.H. Wang, et al., Anal. Chem. 92 (2020) 14769–14774.
[20] S.Y. Liang, S.Y. Li, Y.N. Zhang, et al., Adv. Funct. Mater. 31 (2021) 2102764.
[21] L.P. Duan, M.R.He Y.Zhang, et al., ACS Appl. Mater. Interfaces 12 (2020) 27433–27442.
[22] M.R. Ren, G.C. Zhang, Z. Chen, et al., ACS. Appl. Mater. Interfaces 12 (2020) 13077–13086.
[23] L. Perdigón-Toro, H.T. Zhang, A. Markina, et al., Adv. Mater. 32 (2020) 1906763.
[24] R. Wang, C.F. Zhang, Q. Li, et al., J. Am. Chem. Soc. 142 (2020) 12751–12759.
[25] X.J. Li, R.J. Ma, T. Liu, et al., Sci. China. Chem. 63 (2020) 1256–1261.
[26] Q.P. Fan, Y. Wang, M.J. Zhang, Adv. Mater. 30 (2018) 1704546.
[27] Q. Guo, Q. Guo, Y.F. Geng, Mater. Chem. Front. 5 (2021) 3257–3280.
[28] J. Yuan, Y.Q. Zhang, L.Y. Zhou, et al., Joule 3 (2019) 1140–1151.
[29] R.N. Yu, G.Z. Wu, Z.A. Tan, J. Energy. Chem. 61 (2021) 29–46.
[30] X.M. Zhao, L.Y. Zen, N. Hosmane, et al., Chin. Chem. Lett. 30 (2019) 87–89.
[31] C.Y. Wen, L.L. Wu, Z.L. Zhang, et al., ACS Nano 8 (2014) 941–949.
[32] C.C. Shen, S.P. Liu, X.Q. Li, et al., Anal. Chem. 91 (2019) 11614–11619.
[33] J.J. Luo, D. Liang, D. Zhao, et al., Biosens. Bioelectron. 151 (2020) 111976.
[34] S.X. Liu, B. Yu, S. Wang, et al., Adv. Colloid. Interface. 281 (2020) 102165.